Exploring the anti-oxidative mechanisms of *Rhodiola rosea* in ameliorating myocardial fibrosis through network pharmacology and *in vitro* experiments

LUNA ZHANG[1*], HANG YIN[2*], YUMIN XIE[1*], YUEYUE ZHANG[1], FEIHONG DONG[1], KE WU[1], LE YANG[1] and HUIYI LV[1]

[1]Department of Pharmacy, The Second Affiliated Hospital of Dalian Medical University, Dalian, Liaoning 116023, P.R. China; [2]Institute for Computational Biomedicine, Weill Cornell Medicine, New York, NY 10021, USA

Received May 31, 2024; Accepted September 2, 2024

DOI: 10.3892/mmr.2024.13338

Abstract. Myocardial fibrosis (MF) significantly compromises cardiovascular health by affecting cardiac function through excessive collagen deposition. This impairs myocardial contraction and relaxation and leads to severe complications and increased mortality. The present study employed network pharmacology and *in vitro* assays to investigate the bioactive compounds of *Rhodiola rosea* and their targets. Using databases such as HERB, the Encyclopedia of Traditional Chinese Medicine, Pubchem, OMIM and GeneCards, the present study identified effective components and MF-related targets. Network analysis was conducted with Cytoscape to develop a Drug-Ingredient-Target-Disease network and the STRING database was utilized to construct a protein-protein interaction network. Key nodes were analyzed for pathway enrichment using Gene Ontology and Kyoto Encyclopedia of Genes and Genomes. Molecular interactions were further explored through molecular docking techniques. The bioactivity of salidroside (SAL), the principal component of *Rhodiola rosea*, against MF was experimentally validated in H9c2 cardiomyocytes treated with angiotensin II and assessed for cell viability, protein expression and oxidative stress markers. Network pharmacology identified 25 active ingredients and 372 targets in *Rhodiola rosea*, linking SAL with pathways such as MAPK, EGFR, advanced glycosylation end products-advanced glycosylation end products receptor and Forkhead box O. SAL showed significant interactions with core targets such as albumin, IL6, AKT serine/threonine kinase 1, MMP9 and caspase-3. *In vitro*, SAL mitigated AngII-induced increases in collagen I and alpha smooth muscle actin protein levels and oxidative stress markers, demonstrating dose-dependent effectiveness in reversing MF. SAL from *Rhodiola rosea* exhibited potent anti-oxidative properties that mitigated MF by modulating multiple molecular targets and signaling pathways. The present study underscored the therapeutic potential of SAL in treating oxidative stress-related cardiovascular diseases.

Correspondence to: Professor Huiyi Lv or Dr Le Yang, Department of Pharmacy, The Second Affiliated Hospital of Dalian Medical University, 467 Zhongshan Road, Dalian, Liaoning 116023, P.R. China
E-mail: huiyi-l@dmu.edu.cn
E-mail: yl0520@dmu.edu.cn

*Contributed equally

Abbreviations: AKT1, AKT serine/threonine kinase 1; ALB, albumin; AngII, angiotensin II; BP, biological processes; CASP3, caspase-3; CC, cellular components; COL, collagen; DMEM, Dulbecco's modified Eagle's medium; ETCM, Encyclopedia of Traditional Chinese Medicine; GO, gene ontology; GSH, glutathione; KEGG, Kyoto Encyclopedia of Genes and Genomes; MDA, malondialdehyde; MF, myocardial fibrosis; MTT, methylthiazolyl tetrazolium; PPI, protein-protein interaction; ROS, reactive oxygen species; RT-qPCR, reverse transcription-quantitative PCR; SAL, salidroside; α-SMA, alpha smooth muscle actin.

Key words: network pharmacology, *Rhodiola rosea*, salidroside, oxidative stress, myocardial fibrosis

Introduction

Myocardial fibrosis (MF) plays a critical role in the progression of cardiovascular diseases towards heart failure, often manifesting as cardiac systolic and diastolic dysfunction, arrhythmias and adverse cardiovascular events (1,2). Driven predominantly by coronary atherosclerosis and prolonged myocardial ischemia and hypoxia, MF involves substantial deposition of extracellular matrix components, including collagen (COL) I and COL III (3,4). Such excessive COL production disrupts cardiac function, potentially leading to myocardial infarction and heart failure, thereby posing severe risks to human health (5,6). Traditional therapies such as angiotensin-converting enzyme inhibitors and β-blockers are known to improve ventricular remodeling and enhance blood flow at ischemic sites, offering modest benefits in managing MF. However, the mechanisms of action of these agents are complex and their prolonged use is often associated with significant adverse effects, such as hypotension, dyspnea, bradycardia and shock (7).

Traditional Chinese medicine, with its multifaceted approach encompassing multiple components, pathways and targets, offers unique advantages in both the prevention and treatment of MF (8). Herbal treatments such as *Astragalus* (9), *Salvia miltiorrhiza* (10) and turmeric (11) are known to modulate collagen synthesis, prevent extracellular matrix collagen deposition and mitigate ventricular remodeling, showing potential therapeutic effects against MF. For example, research by Wang *et al* (12) demonstrated that Buyang Huanwu Decoction could attenuate MF by reducing the expression of inflammatory factors and influencing the IL-17 signaling pathway.

Rhodiola rosea, a member of the Crassulaceae family, is known for its diverse beneficial effects including anti-ischemia, anti-oxidation, anti-inflammation, as well as its ability to enhance lung function and relieve asthma (13,14). Notably, it is recognized for its cardiovascular benefits, particularly its capacity to protect cardiovascular endothelial cells and inhibit platelet aggregation (15). Salidroside (SAL), a key active component of *Rhodiola rosea*, has demonstrated properties that alleviate oxidative stress and improve MF. Studies, such as those by Ye *et al* (16), have shown that SAL can mitigate carbon tetrachloride-induced liver fibrosis in mice by inhibiting SK-HEP-1 exosome SphK1, which may reduce liver damage and enhance recovery from liver fibrosis. These findings suggest that *Rhodiola rosea* could similarly exert a protective effect against MF.

The present study examined SAL, the principal active ingredient in *Rhodiola rosea*, for its therapeutic potential against MF related to oxidative stress, identified using network pharmacology techniques. In addition, cell experiments were used to elucidate the effect and mechanism of SAL in the treatment of MF.

Materials and methods

Network pharmacology-related database and software. The present study used various databases and software to identify and analyze the bioactive components of *Rhodiola rosea*, including: HERB database (http://herb.ac.cn/), Encyclopedia of Traditional Chinese Medicine (ETCM) (http://www.tcmip.cn/ETCM/), PubChem database (http://pubchem.ncbi.nlm.nih.gov/), Swiss TargetPrediction (http://swisstargetprediction.ch/), STRING protein interactions information website (http://string-db.org/), GeneCards database (https://www.gege-cards.org/), OMIM database (http://omim.org/), DAVID database (http://david.ncifcrf.gov/summary.jsp), Cytoscape 3.9.1 software (http://cytoscape.org/), Wei Sheng Xin online mapping website (https://www.bioinformatics.com.cn/), Protein Data Bank database (http://www.rcsb.org/), AutoDock Tools 1.5.6 software (https://autodock.scripps.edu/), PyMOL 2.3.6 software (https://pymol.org/), OpenBabel 2.4.1 software (https://openbabel.org/), GraphPad Prism 9.4.1 software (Dotmatics), CytoNCA plugin (https://apps.cytoscape.org/apps/cytonca), and Image Lab 6.0.1 (Bio-Rad Laboratories, Inc.).

Network pharmacology research methods

Screening of active components of Rhodiola and corresponding targets. Active ingredients from *Rhodiola rosea* were identified using the HERB database and the ETCM resource, employing screening criteria based on physicochemical properties: Molecular weight ≤500, logP ≤5, hydrogen bond donors ≤5 and hydrogen bond acceptors ≤10. Selected compounds were saved in simplified molecular input line entry specification (SMILES) format and imported into the SwissTargetPrediction database. Predictions were restricted to human research species with a prediction probability >0. Compounds that did not target any relevant proteins were excluded, resulting in the construction of a comprehensive component-target database for *Rhodiola rosea*.

Target collection and common target screening for oxidative stress and myocardial fibrosis. Using the GeneCards database, genes associated with MF were identified with the keywords 'myocardial fibrosis', selecting targets with a correlation score ≥ the second median. Genes related to oxidative stress were sourced using the keywords 'oxidative stress', selecting those with correlation scores ≥ the third median. The two sets were collated using the OMIM database. Duplicate targets were removed, leading to a refined prediction target library. The target proteins of *Rhodiola rosea* were intersected with disease targets using Wei Sheng Xin online mapping website, identifying shared targets visualized in a Venn diagram.

Construction and analysis of drug-component-target-disease network. A comprehensive drug component-target-disease network was created using Cytoscape 3.9.1 to visualize the interactions between active compounds of *Rhodiola rosea* and their potential targets in combating oxidative stress and MF. The network featured purple nodes for bioactive components and pink nodes for potential targets, with edges representing their interactions.

PPI network construction and analysis. A total of 91 potential targets of the antioxidant properties of SAL against MF were imported into the STRING database. The data were filtered by selecting '*Homo sapiens*' as the organism with a minimum interaction score of ≥0.4. The resulting .tsv file was then imported into Cytoscape 3.9.1, where the CytoNCA plugin was used to compute the degree of each target, enabling the construction of a protein interaction network graph.

Gene ontology (GO) and Kyoto Encyclopedia of Genes and Genomes (KEGG) enrichment analysis. GO function and KEGG signal pathway enrichment analyses were performed using the DAVID database. Results were visualized using the Wei Sheng Xin online mapping website, drawing bar charts for GO function enrichment and bubble charts for KEGG pathway analysis.

Molecular docking analysis of core target and drug active ingredient. Molecular docking was used to evaluate the direct binding interaction between the key active ingredient, SAL, and core targets. Structural formulas and 3D structure files were sourced from the PubChem and the Protein Data Bank databases, respectively. Specific conditions applied to the docking simulations included: Biological Source: *Homo sapiens*; Experimental Method: X-ray diffraction; Resolution: ≤3Å. Using AutoDock Tools 1.5.6 and OpenBabel 2.4.1 software, docking simulations were performed and binding positions and energies were calculated. Structures were visualized with PyMOL 2.3.6 to generate 3D images.

Cell culture and treatment. H9c2 cells (American Type Culture Collection) were cultured in Dulbecco's modified

Eagle's medium (DMEM; Gibco; Thermo Fisher Scientific, Inc.), supplemented with 10% fetal bovine serum (TransGen Biotech Co., Ltd.). Cultures were incubated at 37˚C in a 5% CO_2 atmosphere. To minimize contamination, cultures were treated with a combination of penicillin-streptomycin-gentamicin (100X; cat. no. P1410-100ml; Beijing Solarbio Science & Technology Co., Ltd.) and a separate penicillin-streptomycin solution (100X; cat. no. P1400-100ml; Beijing Solarbio Science & Technology Co., Ltd.).

Methylthiazolyl tetrazolium (MTT) assay. Cells were seeded at a density of $5.0x0^4$ cells per ml in a 96-well plate and exposed to various concentrations of AngII (0.01, 0.1 and 1 μM) in the presence of SAL (50, 100 and 150 μM) dissolved in DMEM for 24 h. Following incubation at 37˚C for 4 h, 50 μl of MTT solution was added to each well. Following a further 4-h incubation at 37˚C, the medium was aspirated and the wells were washed with PBS. Subsequently, 150 μl of dimethyl sulfoxide was added to solubilize the formazan crystals. The optical density (OD) at 570 nm was measured using a SpectraMax 190 microplate reader (Anthos Labtec Instruments GmbH).

Immunofluorescence assay. H9c2 cells were seeded in 24-well plates with slides at a density of $1x10^5$ cells/ml and divided into three treatment groups: Control, 1 μM AngII and 150 μM SAL. After 24 h of treatment, cells were fixed with 4% paraformaldehyde for 15 min at room temperature and washed three times with PBS. Cells were permeabilized with 0.5% Triton-X for 20 min at room temperature, followed by three PBS washes. Wells were blocked with 5% goat serum (Beyotime Institute of Biotechnology) in PBS for 1 h at room temperature. Then, the cells were incubated overnight at 4˚C with 100 μl primary antibody against COL III (1:100; cat. no. A3795; ABclonal Biotech Co., Ltd.). After washing three times with PBS, the cells were incubated with FITC-conjugated Goat anti-Rabbit lgG (H+L) secondary antibody (1:100 dilution; cat. no. AS011; ABclonal Biotech Co., Ltd.) for 1 h at room temperature, incubated with 10 μl DAPI (Beyotime Institute of Biotechnology) at room temperature for 10 min and visualized under a DMI8 inverted fluorescence microscope (Leica Microsystems GmbH) at magnification, x20. The secondary antibody conjugate was FITC; the excitation wavelength was adjusted to 491 nm and FITC was detected under a DMI8 inverted fluorescence microscope at 516 nm (emission) according to the manufacturer's instructions.

Cellular RNA and reverse transcription-quantitative (RT-q) PCR. Cells were seeded in 6-well plates at $2x10^5$ cells/ml and treated with drugs for 24 h. Post-treatment, cells were washed twice with PBS and RNA was extracted using EZol reagent (Shanghai GenePharma Co., Ltd.). RNA quality and quantity were assessed using a Nanodrop quantitative nucleic acid analyzer (Thermo Fisher Scientific, Inc.). cDNA was synthesized from RNA using Hifair III 1st Strand cDNA Synthesis SuperMix for qPCR (Shanghai Yeasen Biotechnology Co., Ltd.). qPCR was performed with Hieff UNICON Universal Blue qPCR SYBR Green Master Mix (Shanghai Yeasen Biotechnology Co., Ltd.). Cycling conditions were 95˚C for 30 sec, followed by 40 cycles of 95˚C for 5 sec and 60˚C for 30 sec. RNA extraction, cDNA synthesis and qPCR were performed according to the manufacturers' protocols, and the experiment was repeated at least three times. β-actin served as the internal reference and relative gene expression was calculated using the $2^{-\Delta\Delta Cq}$ method (17). Primer sequences for IL-6, MMP9, AKT serine/threonine kinase 1 (AKT1), albumin (ALB), caspase-3 (CASP3) and β-actin are given in Table SI.

Western blotting. Cells were lysed in RIPA buffer (Beyotime Institute of Biotechnology) containing phenylmethanesulfonyl fluoride to extract proteins. Protein concentration was determined using a BCA protein assay kit (Beyotime Institute of Biotechnology). Proteins (26 μg) were separated by 7.5% SDS-PAGE (Shanghai Yamei Biotechnology Co. Ltd.) and transferred to PVDF membranes (MilliporeSigma). Membranes were blocked with 5% skimmed milk for 1 h at room temperature, then incubated with primary antibodies against COL I (1:1,000; cat. no. 14695-1-AP; Wuhan Proteintech Biotechnology), alpha smooth muscle actin (α-SMA; 1:1,000; cat. no. A17910; ABclonal Biotech Co., Ltd.) and GAPDH (1:5,000; cat. no. ab181602; Abcam) overnight at 4˚C. After washing, membranes were incubated with HRP-conjugated secondary antibody (1:10,000; cat. no. RGAR001; Wuhan Proteintech Biotechnology) for 1 h at room temperature and developed using an enhanced chemiluminescence substrate (Tanon Science and Technology Co., Ltd.) and ChemiDoc XRS+ Highly Sensitive Chemiluminescence Imaging System (Bio-Rad Laboratories, Inc.). COL I, α-SMA and GAPDH were 139, 42 and 36 kDa, respectively. Image Lab 6.0.1 was used to semi-quantify the blots.

Reactive oxygen species (ROS) level detection by immunofluorescence assay. Cells were directly inoculated into 24-well plates at $1x10^5$ cells/ml and were divided into a control group, 1 μM AngII group and 150 μM SAL group. The cells were treated with the indicated drugs for 24 h. Post-treatment, cells were incubated with DCFH-DA (10 μmol/l) for 30 min at 37˚C. Cells were then washed and visualized under a DMI8 inverted fluorescence microscope (Leica Microsystems GmbH) at x10 magnification.

Determination of malondialdehyde (MDA) content. MDA levels were measured using an MDA assay kit (Beyotime Institute of Biotechnology) after treating cells in 6-well plates at $2x10^5$ cells/ml for 24 h. The working solution from the MDA kit was heated and the absorbance was read at 532 nm on a SpectraMax microplate reader (Anthos Labtec Instruments GmbH).

Glutathione (GSH) content determination. GSH levels were assessed using a GSH assay kit (Beijing Solarbio Science & Technology Co., Ltd.). Cells were sonicated at 200 W at 4˚C, they were sonicated for 3 sec, then stopped for 10 sec, and this was repeated 30 times. The supernatants were collected for analysis after centrifugation of 8,000 x g for 10 min at 4˚C.

Flow cytometry. ROS levels were measured using a ROS assay kit (Beijing Solarbio Science & Technology Co., Ltd.). Post-treatment, cells were incubated with DCFH-DA, washed and analyzed on an Agilent flow cytometer (Agilent Technologies, Inc.).

Table I. Basic information on the chemical composition of *Rhodiola rosea*.

Number	Compound name	Molecular formula	CAS number
1	1,8-menthadien-4-ol	$C_{10}H_6O$	3419-02-1
2	1-octanol	$C_8H_{18}O$	111-87-5
3	1-octen-3-ol	$C_8H_{16}O$	3391-86-4
4	3-methyl-2-buten-1-ol	$C_5H_{10}O$	556-82-1
5	3-methyl-2-butenal	C_5H_8O	107-86-8
6	3-octanol	$C_8H_{18}O$	589-98-0
7	6-methyl-5-hepten-2-ol	$C_8H_{16}O$	1569-60-4
8	6-methyl-5-hepten-2-one	$C_8H_{14}O$	110-93-0
9	Benzeneethanol	$C_8H_{10}O$	60-12-8
10	Formic acid hexyl ester	$C_7H_{14}O_2$	629-33-4
11	Hexanal	$C_{25}H_{44}N_{14}O_8$	2610-10-8
12	Limonene oxide	$C_{10}H_{16}O$	1195-92-2
13	Linalool	$C_{10}H_{18}O$	78-70-6
14	Linalool oxide	$C_{10}H_{18}O_2$	34995-77-2
15	Myrtanol	$C_{10}H_{18}O$	514-99-8
16	Myrtenol	$C_{10}H_{16}O$	515-00-4
17	Octanal	$C_8H_{16}O$	124-13-0
18	Octanoic acid	$C_8H_{16}O$	124-07-2
19	Salidroside	$C_{14}H_{20}O_7$	78-70-6
20	7-hydroxycoumarin	$C_9H_6O_3$	93-35-6
21	Caffeic acid	$C_9H_8O_4$	501-16-6
22	Kaempferol	$C_{15}H_{10}O_6$	520-18-3
23	Gallic acid	$C_7H_6O_5$	149-91-7
24	Ethyl gallate	$C_9H_{10}O_5$	831-61-8
25	Tyrosol	$C_8H_{10}O_2$	501-94-0

Statistical analysis. Statistical analyses were performed using GraphPad Prism 9.4.1 software (Dotmatics). Differences were assessed using one-way ANOVA followed by Bonferroni post hoc test as appropriate. Results are expressed as mean ± standard deviation and $P<0.05$ was considered to indicate a statistically significant difference.

Results

Establishment of a Rhodiola rosea database and visualization of the drug-active ingredient relationship network diagram. Using the HERB and ETCM databases, the present study identified 25 unique ingredients, listed in Table I. The 2D structures and CAS numbers of these components were retrieved from the PubChem database and imported into the SwissTargetPrediction database, resulting in the identification of 312 individual targets. The present study then compiled a comprehensive dataset of targets relating to oxidative stress and MF, gathering 12,835 oxidative stress-related targets from the GeneCards database. Of these, 1,242 targets had correlation scores above the median value and 5,090 targets were specifically linked to MF. From this subset, the present study isolated 1,667 targets with correlation scores above the third median. Using a Venn diagram, the overlap between *Rhodiola rosea* targets and those related to oxidative stress and MF was visualized, identifying 157 intersecting targets as potential mediators of the effects of *Rhodiola rosea* (Fig. 1A). Employing Cytoscape 3.9.1 software, a drug-component-target-disease network diagram was created (Fig. 1B). Using CytoNCA, the present study furthered identified the top five active ingredients based on their degree ranking: SAL, kaempferol, β-sitosterol, tanshinone IIA and ginsenoside Rh2 (Table II). Notably, SAL was the primary component that mitigated MF through its antioxidant properties. The potential targets of *Rhodiola rosea*'s SAL component for counteracting MF were subsequently imported into the STRING protein interaction database, which enabled it to identify 91 protein nodes and 586 interaction edges, with a local clustering coefficient of 0.602 and a PPI enrichment P-value of $<1.0\times10^{-16}$. After importing the data into Cytoscape and using the CytoNCA plugin, the protein interaction network was visualized and the top 32 core interaction targets identified for further analysis (Fig. 1C and D). The primary five core targets were identified as serum ALB (Degree=81.0), IL6 (Degree=71.0), AKT1 (Degree=68.0), MMP9 (Degree=59.0) and CASP3 (Degree=57.0). Using the DAVID database, these targets were analyzed and 317 biological processes (BP), 52 cellular components (CC) and 76 molecular functions (MF) predominantly involved in the negative regulation of apoptosis, protein hydrolysis and cell proliferation were identified (Fig. 1E). Additionally, 142 KEGG pathways enriched at $P<0.05$ were identified, highlighting the top 20 signaling pathways involved in the cardioprotective

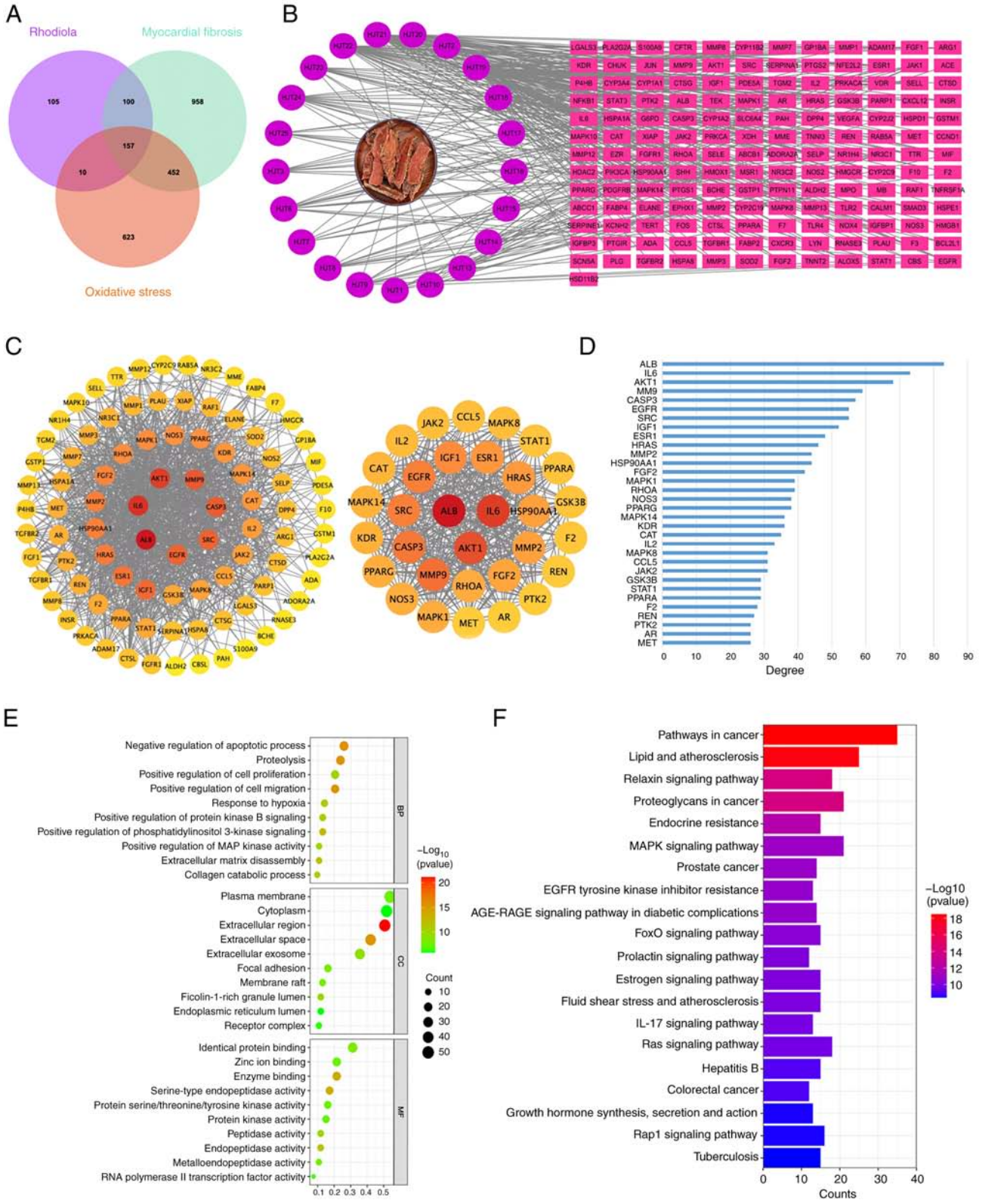

Figure 1. Role of *Rhodiola rosea* in mitigating myocardial fibrosis through antioxidative stress mechanisms employing network pharmacology. (A) Venn diagram of intersection targets of *Rhodiola* antioxidative stress in improving myocardial fibrosis. (B) Drug-component-target-disease network. (C) STRING protein interaction network (D) Visualization histogram of top 32 intersection targets of *Rhodiola*. (E) GO enrichment analysis of core targets. (F) KEGG pathway enrichment analysis of core targets. STRING, Search Tool for the Retrieval of Interacting Genes; GO, gene ontology; KEGG, Kyoto Encyclopedia of Genes and Genomes.

effects mediated by SAL (Fig. 1F). This analysis highlighted the role of SAL in regulating crucial cellular processes such as cell proliferation, apoptotic processes and inflammation and its involvement in cardiovascular and metabolic pathways associated with conditions such as cancer, atherosclerosis and diabetes complications.

Table II. Top five Chinese medicine components in the degree network diagram of drug component target disease.

Ranking	Components	Degree:score
1	Salidroside	14.0
2	Kaempferol	9.0
3	β-sitosterol	7.0
4	Tanshinone IIa	6.0
5	Ginsenoside Rh2	6.0

These findings provided valuable insights into the underlying mechanisms of the cardioprotective actions of *Rhodiola rosea*, emphasizing SAL as the key active ingredient in combating MF through its antioxidant capabilities.

Molecular docking analysis. Molecular docking was performed following the preparation of the target protein using AutoDock Tools 1.5.6. SAL and its corresponding core target molecules were docked to evaluate the binding efficacy. Adjustments were made to the mesh size to optimize the analysis of binding positions and docking energies. Binding energies were found to be <-1.2 kcal/mol, indicating a strong potential for binding between the drug and its targets. Specifically, a binding energy <0 kcal/mol suggests a favorable binding interaction, with values ≤-1.2 kcal/mol indicating effective docking and potential therapeutic efficacy. Lower binding energies denoted increased stability and a higher likelihood of a successful interaction between the ligand and the receptor. From a molecular perspective, these results supported the potential therapeutic effects of SAL on MF, given its robust interactions with key molecular targets such as ALB, IL6, AKT1, MMP9 and CASP3 in Table III. Fig. 2 illustrates the 3D interaction model between SAL and the core target molecules, underscoring the potential mechanism by which SAL may inhibit MF in H9c2 cells through these key interactions.

Efficacy of SAL in ameliorating myocardial fibrosis. To evaluate the effect of various concentrations of AngII and SAL on H9c2 cardiomyocyte viability after 24 h of treatment, an MTT assay was employed. The results demonstrated that incubating H9c2 cells with 0.01, 0.1 and 1 μM AngII did not significantly alter cell viability (Fig. 3A). Similarly, treatment with SAL at concentrations of 50, 100 and 150 μM did not affect cell viability (Fig. 3B). Then, the cells were treated with 0.01, 0.1 and 1 μM AngII for 24 h to verify whether AngII induced MF successfully. Subsequent western blotting revealed a dose-dependent increase in the levels of COL I and α-SMA, which are biomarkers indicative of MF (3,18), following 24 h of exposure to AngII. This dose-dependent increase confirmed the successful establishment of the MF model with AngII, particularly with significant elevations in both COL I and α-SMA levels in the 1 μM AngII group compared with lower concentrations (P<0.01; Fig 3C). AngII at 1 μM was the most significant in establishing MF model. Further experiments employed H9c2 cells treated with 1 μM AngII for 24 h as the MF model. The next step was to verify the therapeutic effect of different concentrations of SAL on MF. Cells were pre-treated with 1 μM AngII for 2 h before adding SAL at 50, 100 and 150 μM concentrations and co-incubating for an additional 24 h. Western blotting was conducted to assess changes in COL I and α-SMA levels. Results indicated a dose-dependent reduction in these fibrosis markers in the SAL treatment groups, demonstrating the capacity of SAL to effectively reverse AngII-induced MF. Notably, the levels of both COL I and α-SMA were significantly lower in the 150 μM SAL group compared with lower concentrations of SAL, highlighting the robust therapeutic potential of SAL at higher doses (P<0.001; Fig. 3D). This evidence substantiated the therapeutic efficacy of SAL in reducing MF markers, suggesting its potential utility as a treatment option in MF management.

Salidroside mitigates myocardial fibrosis through multi-target mechanisms. For subsequent experiments, the present study established a treatment regimen where H9c2 cells were exposed to 150 μM SAL for 24 h as the primary drug treatment group. Simultaneously, another set of cells were treated with 1 μM AngII alone, followed by an additional 24-h treatment with 150 μM SAL. Using immunofluorescence assays, the level of COL III, a well-established marker of MF (4), was assessed. The results showed that 1 μM AngII significantly elevated COL III levels compared with the control group (P<0.05). Notably, treatment with 150 μM SAL markedly reduced COL III levels relative to the AngII-only treated group (P<0.05), illustrating the potent antifibrotic effects of SAL (Fig. 4A). To elucidate the underlying mechanisms of the antifibrotic action of SAL, RT-qPCR was used to verify its effect on multiple targets associated with MF (Fig. 4B). The RT-qPCR results revealed elevated mRNA levels of IL6, MMP9 and CASP3 in the 1 μM AngII group compared with controls, while ALB and AKT1 mRNA levels were significantly decreased. Markedly, treatment with 150 μM SAL not only reduced the mRNA levels of IL6, MMP9 and CASP3 but also increased those of ALB and AKT1 relative to the AngII group. These findings confirmed that SAL counters AngII-induced MF by modulating the expression of critical fibrosis-related genes. The multi-target action of SAL highlighted its potential as a therapeutic agent for the treatment of MF, effectively reversing the pathological processes through interactions with key molecular pathways.

Antioxidative effects of SAL in mitigating myocardial fibrosis. To validate the antioxidative properties of SAL, assessments were conducted on several oxidative stress biomarkers. The MDA assay results showed that MDA levels were significantly elevated in the 1 μM AngII group compared with controls, indicating increased oxidative stress. However, treatment with 150 μM SAL resulted in a notable reduction in MDA levels compared with the 1 μM AngII group (P<0.05), highlighting the ability of SAL to suppress MDA production and counteract oxidative stress induced by AngII (Fig. 5A). Further analysis using a GSH assay revealed a significant decrease in GSH levels in the 1 μM AngII group compared with controls (P<0.05). Conversely, GSH levels were significantly elevated in the 150 μM SAL group compared with the 1 μM AngII group (P<0.05), suggesting that SAL enhanced GSH production, thereby protecting against oxidative stress (Fig. 5B). The basis for assessing the increase in ROS is to

Table III. Molecular docking binding energy of SAL and core targets.

Targets	PDB ID	Ingredients	Pubchem ID	Affinity, kcal/mol
ALB	7VR0	Salidroside	159278	-3.23
IL6	7NXZ	Salidroside	159278	-4.31
AKT1	1UNQ	Salidroside	159278	-3.27
MMP9	6ESM	Salidroside	159278	-3.8
CASP3	1RHJ	Salidroside	159278	-3.11

SAL, salidroside; ALB albumin; AKT1, AKT serine/threonine kinase 1; CASP3, caspase-3.

study the extent of cellular oxidative stress by detecting the levels of ROS within cells. Immunofluorescence and flow cytometry are the commonly used methods. These methods have high sensitivity, high selectivity, high throughput and are non-destructive and can detect trace changes in intracellular ROS without interference from other substances, which can improve experimental efficiency and is suitable for long-term and continuous monitoring. Therefore, immunofluorescence assay and flow cytometry were employed to detect ROS levels. These confirmed that ROS levels were substantially higher in the 1 μM AngII group compared with controls ($P<0.01$). Markedly, the 150 μM SAL group showed a significant decrease in ROS levels compared with the 1 μM AngII group ($P<0.01$ in immunofluorescence and $P<0.05$ in flow cytometry), illustrating the potent antioxidative activity of SAL (Fig. 5C and D). Collectively, these findings demonstrated that SAL effectively inhibited ROS production and enhanced antioxidant defenses in H9c2 cells, thus mitigating AngII-induced oxidative stress. This multifaceted antioxidative response underlined the therapeutic potential of SAL in the treatment of MF.

Discussion

The present study investigated the protective effects of *Rhodiola rosea* against MF-induced cardiac injury and relevant mechanisms. The top five active ingredients of *Rhodiola rosea* against MF via anti-oxidative stress were screened by network pharmacology, and SAL ranked first, indicating that SAL was the main component of *Rhodiola rosea* in its anti-oxidative stress mechanism to improve MF. The PPI network identified the top 32 core interaction targets, among which five key targets ALB, IL-6, AKT1, MMP9 and CASP3 were considered to have high research value. Hence, the principle components of *Rhodiola rosea* are able to play a crucial role in MF through the aforementioned targets. Among 317 BPs, 52 CCs and 76 MFs and 142 KEGG enriched signaling pathways, SAL regulated crucial cellular processes primarily involved in cell proliferation, apoptotic processes and inflammation and demonstrated involvement in cardiovascular and metabolic pathways associated with conditions such as cancer, atherosclerosis and complications in diabetes. The network pharmacology analysis was confirmed by SAL reducing MF markers COL I, COL III and α-SMA levels in H9c2 cells induced by AngII. In parallel, SAL significantly decreased the inflammatory factors IL6, MMP9 and CASP3 levels and suppressed oxidative stress MDA, ROS and increasing GSH expressions, the underlying mechanisms of which might be related to increasing levels of ALB and AKT1.

Network Pharmacology analysis was performed to investigate the bioactive ingredients of the *Rhodiola rosea*. The results demonstrated the top five active constituents were SAL, kaempferol, β-sitosterol, tanshinone IIA and ginsenoside Rh2. These compounds have promising ability in their antioxidant (19), anti-tumor (20) and anti-inflammatory effects (21,22). Additionally, they may suppress AngII-induced inflammatory in atrial fibrosis and atrial fibrillation (23) and cardiotoxicity induced with 5-FU (24). In terms of mitigating MF, SAL was the principle component due to its antioxidant properties. Furthermore, as signaling molecules, these compounds can influence angiogenesis (25) and inhibit apoptosis (26) and pyroptosis (27). SAL has the effects of protecting endothelial barrier disruption induced by intermittent hypoxia and acts against atherosclerosis (28). In addition, SAL enhances anti-apoptosis cardiomyocyte and ventricular remodeling in a cardiomyopathy mouse model (29). Based on the aforementioned findings, the present study was mainly concerned with SAL from *Rhodiola rosea* to observe the critical influence in MF by its anti-oxidant activity.

MF is the hallmark of cardiovascular diseases with regard to heart failure, leading to cardiac systolic and diastolic dysfunction, arrhythmias and adverse cardiovascular events (1,2). MF generates substantial deposition of extracellular matrix components in the cardiac microenvironment (3,4). The present study showed that COL I and COL IIII were abundant in H9c2 cells induced by AngII, illustrating the weakened elasticity of the vascular wall. SAL treatment increased the proportion of COL I and COL IIII, suggesting that SAL partly contributed to the recovery of ventricular compensation. The aforementioned findings showed that SAL alleviated MF, supporting the evidence for the potential of SAL to defeat MF. It has been reported that *Rhodiola* granules significantly strengthen cardiac function and reduce the fibrotic area in an ischemia/reperfusion injury model of rats (30). α-SMA is the marker of mature myofibroblast in cardiac tissues (31). Cardiac fibrosis is normally quiescent, but is activated when triggered by various stimuli and transformed into α-SMA-positive myofibroblasts (32). In the present study, α-SMA levels were markedly upregulated by AngII, while SAL lowered α-SMA levels. A previous study indicated that appropriate activation of myofibroblasts is promising for tissue repair; however, excessively activated myofibroblasts may even result in heart

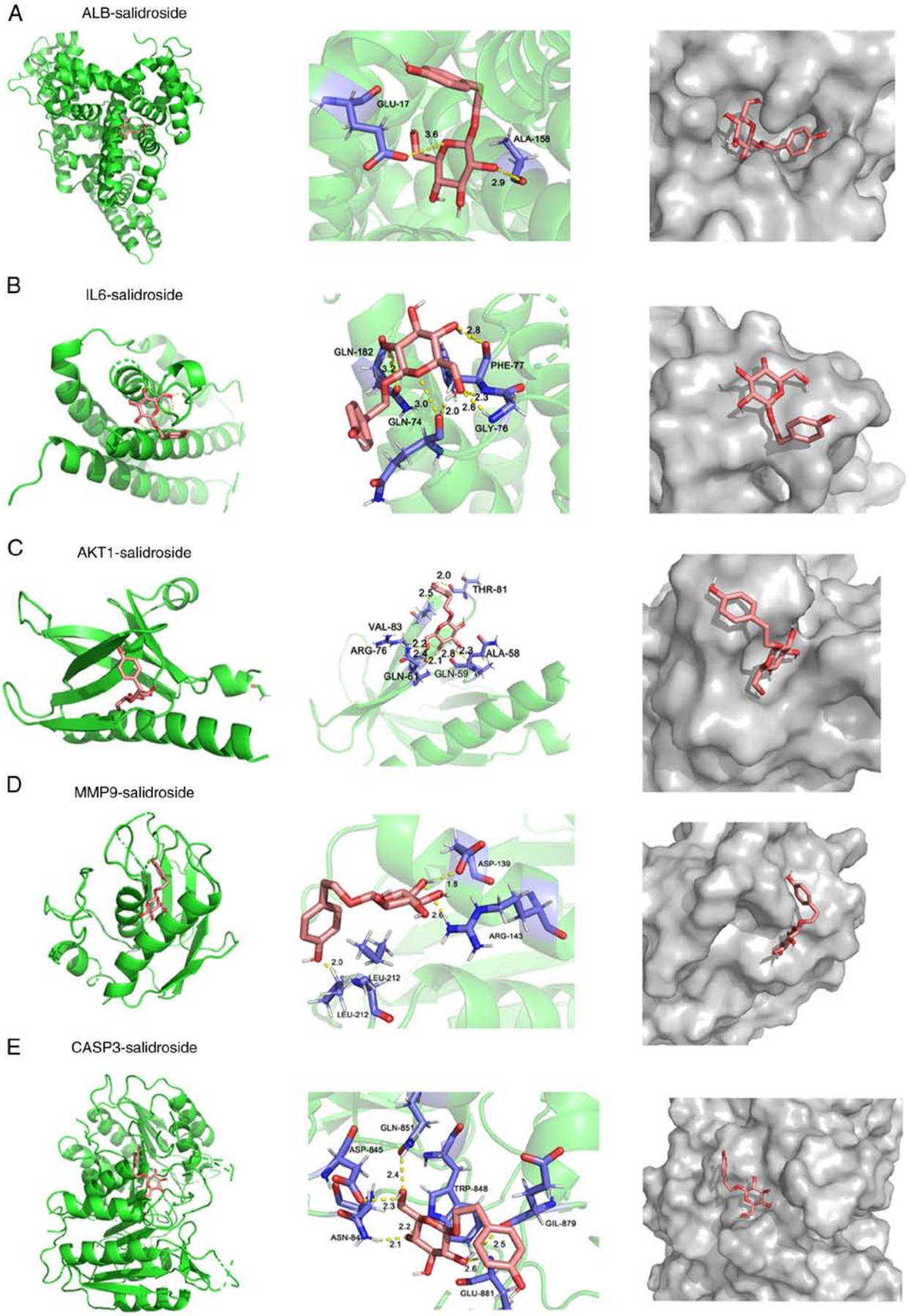

Figure 2. Salidroside treats myocardial fibrosis through multiple targets. Salidroside is represented in pink, core targets are represented in green and grey, linked residues are represented in purple (residue names are represented in text) and hydrogen bonds are represented in yellow dashed lines. (A) ALB and salidroside molecular docking (B) IL6 and salidroside molecular docking. (C) AKT1 and salidroside molecular docking (D) MMP9 and salidroside molecular docking. (E) CASP3 and salidroside molecular docking. ALB, albumin; AKT1, AKT serine/threonine kinase 1; CASP3, caspase-3.

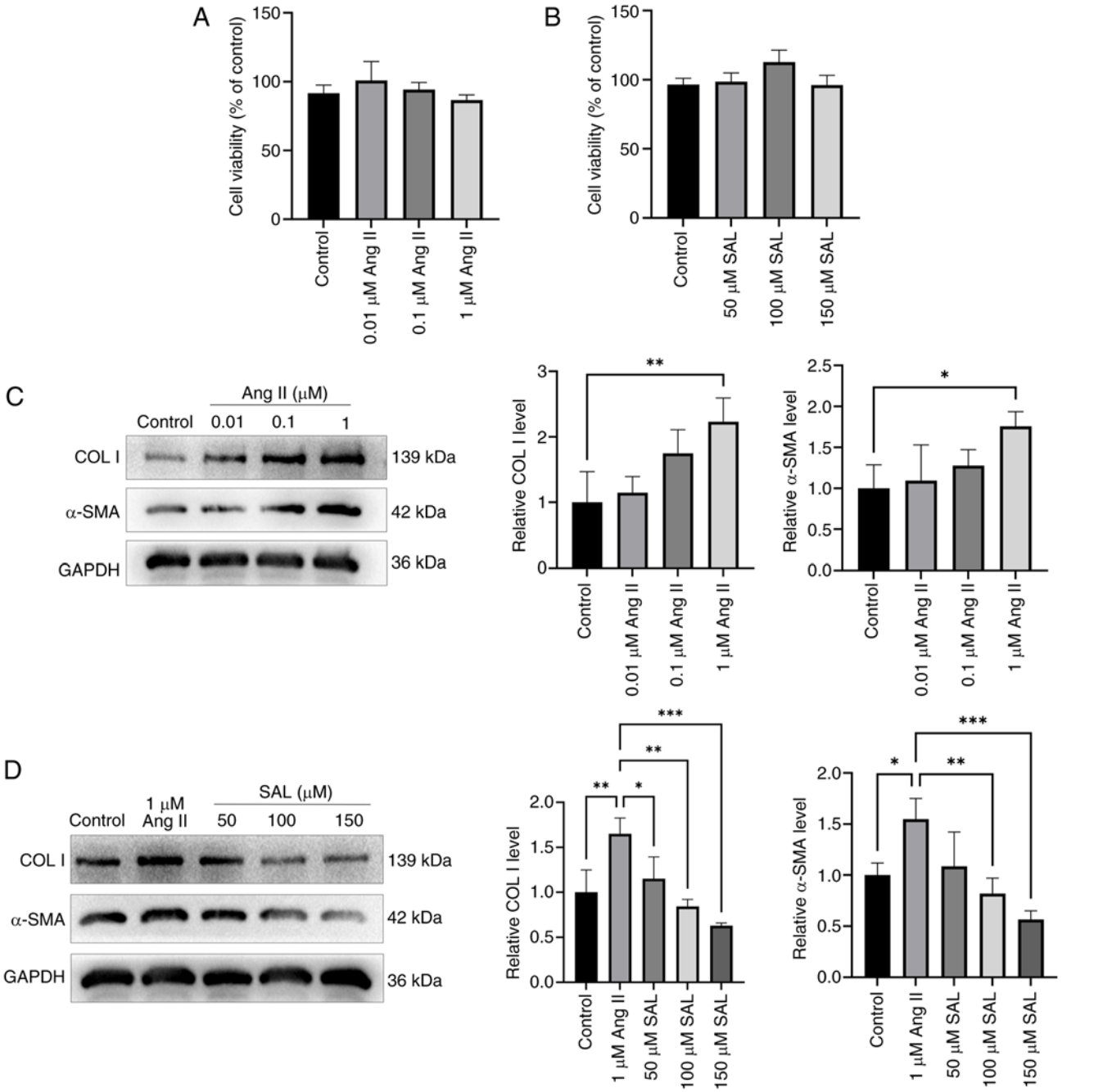

Figure 3. SAL effectively mitigates myocardial fibrosis. (A) The activity of different concentrations of AngII on H9c2 cells by MMT Assay. (B) The activity of different concentrations of SAL on H9c2 cells by MMT Assay. (C) The protein levels of myocardial fibrosis markers COL I and α-SMA induced by AngII were detected by western blotting. (D) The protein levels of myocardial fibrosis markers COL I and α-SMA after SAL treatment by western blotting. *P<0.05, **P<0.01, ***P<0.001. SAL, salidroside; AngII, angiotensin II; MTT, methylthiazolyl tetrazolium; COL, collagen; α-SMA, alpha smooth muscle actin.

failure (33). Yang *et al* (34) found that SAL clearly decreased α-SMA expression in the renal interstitium, which is in line with the data of the present study.

In addition, the anti-inflammatory properties of *Rhodiola* were highlighted. MF is closely associated with inflammation and fibrosis is the last stage of a chronic inflammatory response. IL6 is a proinflammatory cytokine in MF. Fibroblasts maintain this potential pathogenic change by regulating the production of IL6. The results of the present study demonstrated that SAL downregulated IL6 levels. IL6 overexpression induces myofibroblast proliferation, differentiation and fibrosis (1). In addition, SAL downregulated the expressions of MMP9 and CASP3. Hence, SAL prominently reduced pro-inflammatory cytokines, which prolong exacerbation of collagen deposition and MF. Chinese medicinal compounds, including ginsenoside and berberine, have also been shown to offer protective effects against MF by targeting similar pathways, thereby reinforcing the therapeutic potential of natural compounds in cardiac fibrosis management (35,36).

In the data of network pharmacology, the present study found that ALB and AKT1 were also mostly involved in MF. Jäntti *et al* (37) reported that ALB is critical for cardiac function. The results of the present study showed that SAL increased the ALB and AKT1 levels in H9c2 cells treated with

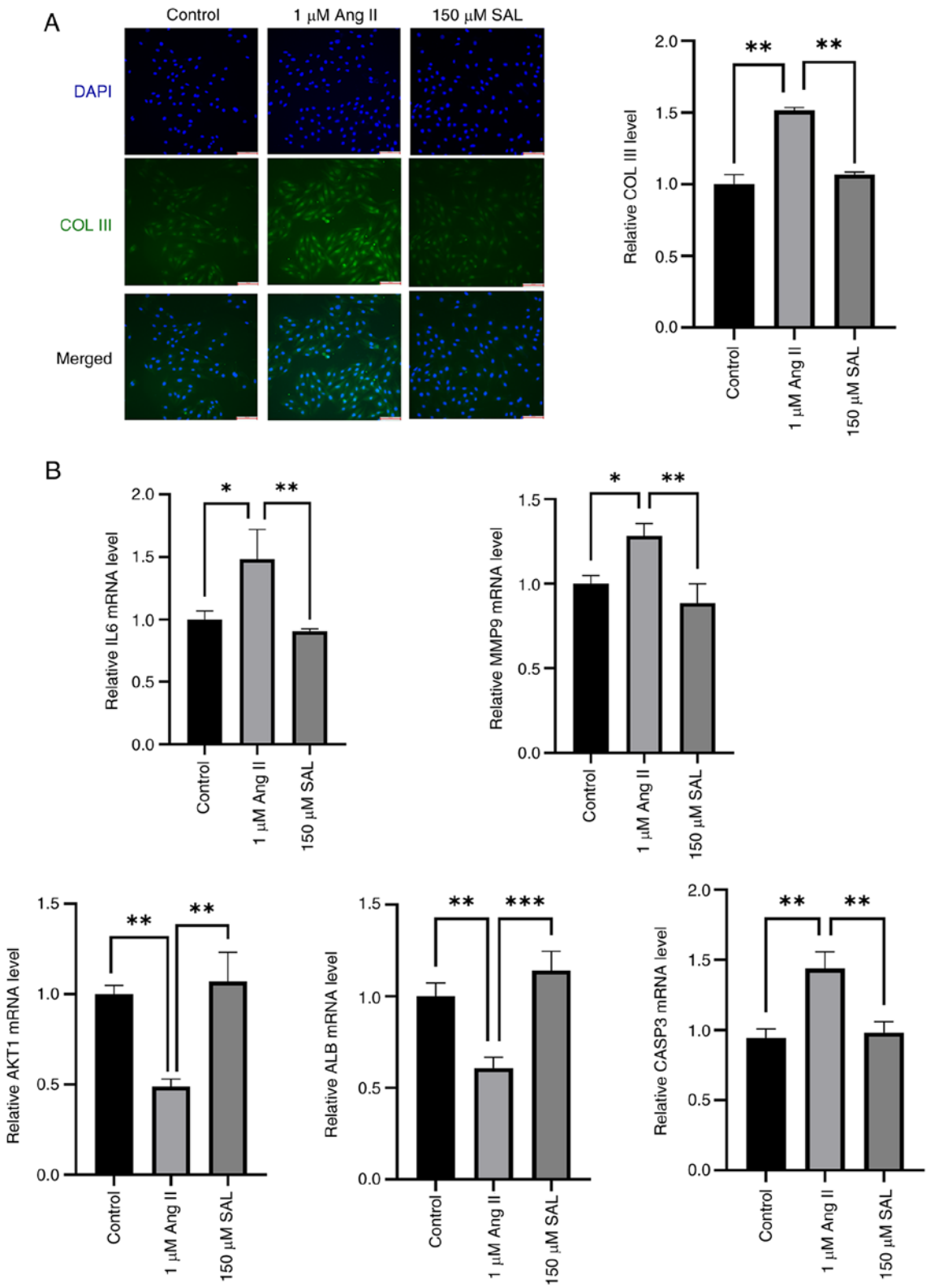

Figure 4. SAL improves myocardial fibrosis through multiple targets. (A) The level of myocardial fibrosis marker COL III by immunofluorescence (magnification, x20; scale bar, 100 μm) (B) The mRNA levels of IL6, MMP9, AKT1, ALB and CASP3 by reverse transcription-quantitative PCR. *P<0.05, **P<0.01 , ***P<0.001. SAL, salidroside; COL, collagen; AKT1, AKT serine/threonine kinase 1; ALB, albumin; CASP3, caspase-3.

AngII. It has been reported that the cardiac function of patients improves with an increase in ALB level and that subsequently their quality of life is improved. The Akt signaling pathway is associated with the cardiac hypertrophy (38). The present study showed that SAL increased AKT1.

The pathogenesis of MF involves complex mechanisms, including the activation of the renin-angiotensin-aldosterone system (RAAS) (39,40), with AngII being a pivotal mediator not only in the cardiovascular system but also in other organs, such as the kidneys and liver. RAAS inhibitors have shown

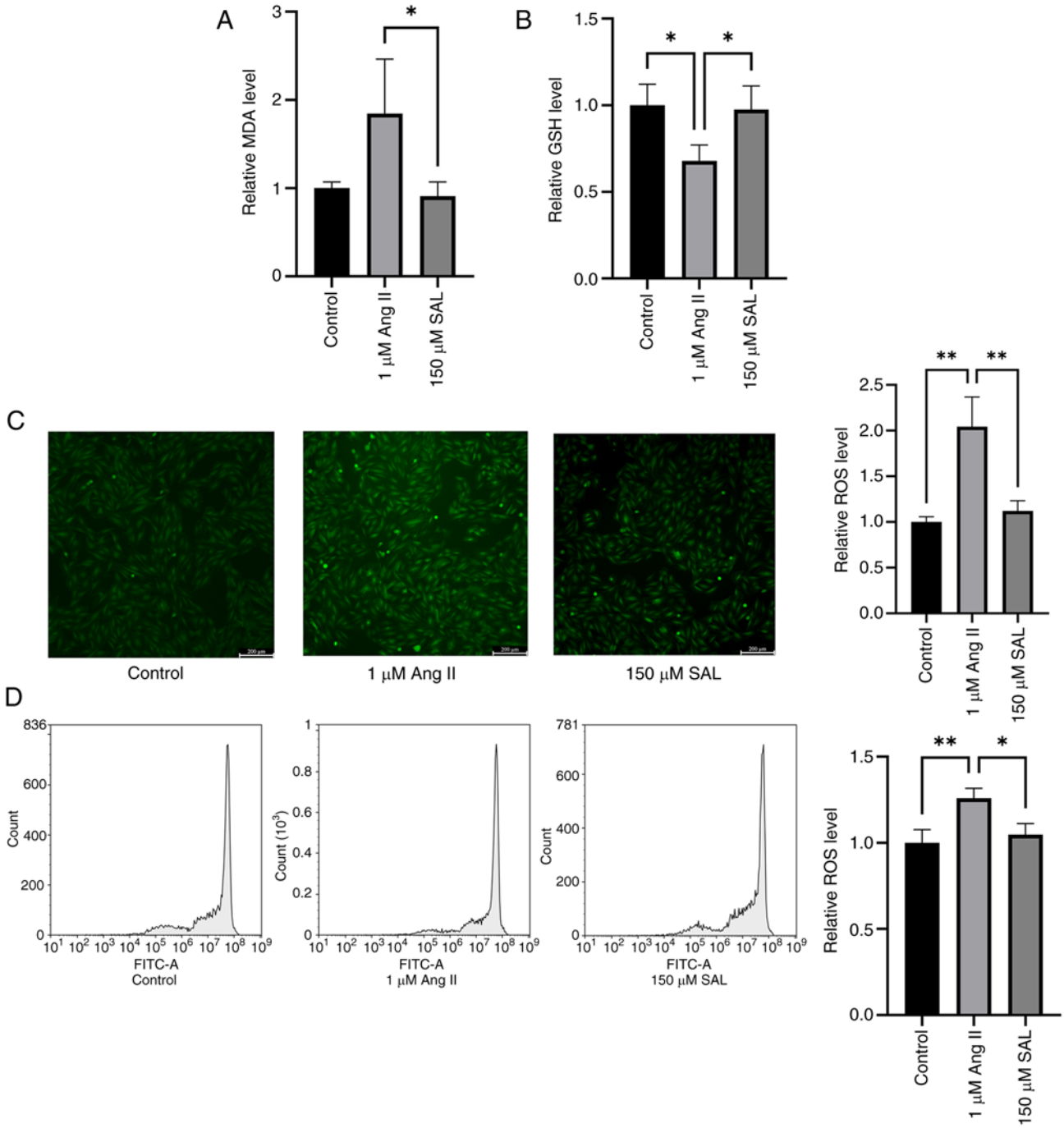

Figure 5. SAL exerts an antioxidative stress effect and thereby mitigates myocardial fibrosis. (A) MDA levels in H9c2 cells (B) GSH levels in H9c2 cells (C, D) ROS levels in H9c2 cells were determined by immunofluorescence and flow cytometry (magnification, x10; scale bar, 200 μm). *P<0.05, **P<0.01. SAL, salidroside; MDA, malondialdehyde; GSH, glutathione; ROS, reactive oxygen species; AngII, angiotensin II.

efficacy in mitigating liver fibrosis and reducing portal hypertension (41), illustrating the broad pathophysiological effect of RAAS. In addition, AngII stimulates fibroblast cell migration and proliferation, enhancing collagen production and contributing to myocardial structural disarray (42).

The present study explored the oxidative stress pathways involved in MF, revealing that AngII intensifies oxidative stress by increasing ROS and MDA levels while reducing GSH levels, indicating an imbalance between pro-oxidant and antioxidant mechanisms. Oxidative stress further triggers pathways leading to cell apoptosis and necrosis, accelerating MF progression. The findings using network pharmacology identified 25 active components in *Rhodiola rosea*, with SAL emerging as a key antioxidant agent. SAL demonstrated significant efficacy in modulating the expression of oxidative and fibrotic markers such as COL I, COL III, α-SMA, IL6, MMP9 and CASP3, underscoring its potential therapeutic benefits in MF treatment.

The present study possessed some limitations. First, it only used H9c2 cells to study the myocardial markers, basic structure and function induced by SAL. It would be more precise to extract rat neonatal cardiomyocytes and determine the effect of SAL on cardiomyocyte activity and proliferation. Second,

the present study used H9c2 cells to explore the effect of SAL on the MF process and the underlying mechanisms associated with fibrosis. In future studies cardiac fibroblast cells should be applied to illustrate the SAL treatments in progress of MF. Third, the present study used immunofluorescence and western blotting to detect the expressions of COL I and COL III. Using RT-qPCR for the detection of COL I and COL III should be in a future study.

In conclusion, the present study elucidated the complex interplay of oxidative stress, inflammation and fibrosis in MF and highlighted the efficacy of *Rhodiola rosea*, particularly SAL, in ameliorating these pathological processes. These insights provided a strong foundation for further development of targeted therapies for MF, using the multifaceted actions of natural compounds to address this debilitating condition.

Acknowledgements

Not applicable.

Funding

The present study was supported by the National Natural Science Foundation of China (grant no. 82304868 for LY) and the Dalian Chinese Medicine Scientific Research Project (grant no. 22Z12006 for HL).

Availability of data and materials

The data generated in the present study may be requested from the corresponding author.

Authors' contributions

HL contributed to the conception and design of the study. LZ and FD conducted data curation and formal analysis. YZ and KW was responsible for sample collection. YX was responsible for data analysis. HY and LY collected data, discussed and revised the manuscript. LZ, HY and YX confirm the authenticity of all the raw data. All authors read and approved the final version of the manuscript.

Ethics approval and consent to participate

Not applicable.

Patient consent for publication

Not applicable.

Competing interests

The authors declare that they have no competing interests.

References

1. Frangogiannis NG: Cardiac fibrosis. Cardiovasc Res 117: 1450-1488, 2021.
2. Karamitsos TD, Arvanitaki A, Karvounis H, Neubauer S and Ferreira VM: Myocardial tissue characterization and fibrosis by imaging. JACC Cardiovasc Imaging 13: 1221-1234, 2020.
3. Talman V and Ruskoaho H: Cardiac fibrosis in myocardial infarction-from repair and remodeling to regeneration. Cell Tissue Res 365: 563-581, 2016.
4. Weber KT, Janicki JS, Shroff SG, Pick R, Chen RM and Bashey RI: Collagen remodeling of the pressure-overloaded, hypertrophied nonhuman primate myocardium. Circ Res 62: 757-765, 1988.
5. Schlittler M, Pramstaller PP, Rossini A and De Bortoli M: Myocardial fibrosis in hypertrophic cardiomyopathy: A perspective from fibroblasts. Int J Mol Sci 24: 14845, 2023.
6. Kong P, Christia P and Frangogiannis NG: The pathogenesis of cardiac fibrosis. Cell Mol Life Sci 71: 549-574, 2013.
7. Roubille F, Busseuil D, Merlet N, Kritikou EA, Rhéaume E and Tardif JC: Investigational drugs targeting cardiac fibrosis. Expert Rev Cardiovasc Ther 12: 111-125, 2014.
8. Luo H, Vong CT, Chen H, Gao Y, Lyu P, Qiu L, Zhao M, Liu Q, Cheng Z, Zou J, *et al*: Naturally occurring anti-cancer compounds: Shining from Chinese herbal medicine. Chin Med 14: 48, 2019.
9. Ren C, Zhao X, Liu K, Wang L, Chen Q, Jiang H, Gao X, Lv X, Zhi X, Wu X and Li Y: Research progress of natural medicine Astragalus mongholicus Bunge in treatment of myocardial fibrosis. J Ethnopharmacol 305: 116128, 2023.
10. Zhang Y, Wang H, Cui L, Zhang Y, Liu Y, Chu X, Liu Z, Zhang J and Chu L: Continuing treatment with salvia miltiorrhiza injection attenuates myocardial fibrosis in chronic iron-overloaded mice. PLoS One 10: e0124061, 2015.
11. Gorabi AM, Hajighasemi S, Kiaie N, Rosano GMC, Sathyapalan T, Al-Rasadi K and Sahebkar A: Anti-fibrotic effects of curcumin and some of its analogues in the heart. Heart Fail Rev 25: 731-743, 2019.
12. Wang T, Jiang X, Ruan Y, Zhuang J and Yin Y: Based on network pharmacology and in vitro experiments to prove the effective inhibition of myocardial fibrosis by Buyang Huanwu decoction. Bioengineered 13: 13767-13783, 2022.
13. Pu WL, Zhang MY, Bai RY, Sun LK, Li WH, Yu YL, Zhang Y, Song L, Wang ZX, Peng YF, *et al*: Anti-inflammatory effects of Rhodiola rosea L.: A review. Biomed Pharmacother 121: 109552, 2020.
14. Gao H, Tian K, Meng Y, Liu X and Peng Y: Salidroside ameliorates cardiomyocyte hypertrophy by upregulating peroxisome proliferator-activated receptor-α. Front Pharmacol 13: 865434, 2022.
15. Chen Y, Tang M, Yuan S, Fu S, Li Y, Li Y, Wang Q, Cao Y, Liu L and Zhang Q: Rhodiola rosea: A therapeutic candidate on cardiovascular diseases. Oxid Med Cell Longev 2022: 1348795, 2022.
16. Ye Q, Zhou Y, Zhao C, Xu L and Ping J: Salidroside inhibits CCl4-induced liver fibrosis in mice by reducing activation and migration of HSC induced by liver sinusoidal endothelial cell-derived exosomal SphK1. Front Pharmacol 12: 677810, 2021.
17. Livak KJ and Schmittgen TD: Analysis of relative gene expression data using real-time quantitative PCR and the 2(-Delta Delta C(T)) method. Methods 25: 402-408, 2001.
18. Hinz B: Myofibroblasts. Exp Eye Res 142: 56-70, 2016.
19. Xu F, Xu J, Xiong X and Deng Y: Salidroside inhibits MAPK, NF-κB, and STAT3 pathways in psoriasis-associated oxidative stress via SIRT1 activation. Redox Rep 24: 70-74, 2019.
20. Fang ZY, Zhang M, Liu JN, Zhao X, Zhang YQ and Fang L: Tanshinone IIA: A review of its anticancer effects. Front Pharmacol 11: 611087, 2020.
21. Yu T, Xu J, Wang Q, Han X, Tu Y, Wang Y, Luo W, Wang M and Liang G: 20(S)-ginsenoside Rh2 inhibits angiotensin-2 mediated cardiac remodeling and inflammation associated with suppression of the JNK/AP-1 pathway. Biomed Pharmacother 169: 115880, 2023.
22. Fan Y, Shen J, Liu X, Cui J, Liu J, Peng D and Jin Y: β-Sitosterol suppresses lipopolysaccharide-induced inflammation and lipogenesis disorder in bovine mammary epithelial cells. Int J Mol Sci 24: 14644, 2023.
23. Hai Z, Wu Y and Ning Z: Salidroside attenuates atrial fibrosis and atrial fibrillation vulnerability induced by angiotensin-II through inhibition of LOXL2-TGF-β1-Smad2/3 pathway. Heliyon 9: e21220, 2023.
24. Safarpour S, Pirzadeh M, Ebrahimpour A, Shirafkan F, Madani F, Hosseini M, Moghadamnia AA and Kazemi S: protective effect of kaempferol and its nanoparticles on 5-fluorouracil-induced cardiotoxicity in rats. Biomed Res Int 2022: 2273000, 2022.
25. Wang Y, Han J, Luo L, Kasim V and Wu S: Salidroside facilitates therapeutic angiogenesis in diabetic hindlimb ischemia by inhibiting ferroptosis. Biomed Pharmacother 159: 114245, 2023.

26. Tang X, Yan T, Wang S, Liu Q, Yang Q, Zhang Y, Li Y, Wu Y, Liu S, Ma Y and Yang L: Treatment with β-sitosterol ameliorates the effects of cerebral ischemia/reperfusion injury by suppressing cholesterol overload, endoplasmic reticulum stress, and apoptosis. Neural Regen Res 19: 642-649, 2024.
27. Song W, Dai B and Dai Y: Influence of ginsenoside Rh2 on cardiomyocyte pyroptosis in rats with acute myocardial infarction. Evid Based Complement Alternat Med 2022: 5194523, 2022.
28. Li L, Yang Y, Zhang H, Du Y, Jiao X, Yu H, Wang Y, Lv Q, Li F, Sun Q and Qin Y: Salidroside ameliorated intermittent hypoxia-aggravated endothelial barrier disruption and atherosclerosis via the cAMP/PKA/RhoA signaling pathway. Front Pharmacol 12: 723922, 2021.
29. Ni J, Li Y, Xu Y and Guo R: Salidroside protects against cardiomyocyte apoptosis and ventricular remodeling by AKT/HO-1 signaling pathways in a diabetic cardiomyopathy mouse model. Phytomedicine 82: 153406, 2021.
30. Xing N, Qin J, Ren D, Du Q, Li Y, Mi J, Zhang F, Ai L, Zhang S, Zhang Y and Wang S: Integrating UPLC-Q-Exactive Orbitrap/MS, network pharmacology and experimental validation to reveal the potential mechanism of Tibetan medicine Rhodiola granules in improving myocardial ischemia-reperfusion injury. J Ethnopharmacol 314: 116572, 2023.
31. Shinde AV, Humeres C and Frangogiannis NG: The role of α-smooth muscle actin in fibroblast-mediated matrix contraction and remodeling. Biochim Biophys Acta Mol Basis Dis 1863: 298-309, 2017.
32. Medarametla GD, Kahlon RS, Mahitha L, Shariff S, Vakkalagadda NP, Chopra H, Kamal MA, Patel N, Sethi Y and Kaka N: Cardiac amyloidosis: Evolving pathogenesis, multimodal diagnostics, and principles of treatment. EXCLI J 22: 781-808, 2023.
33. Argon A, Nart D and Yilmazbarbet F: Cardiac amyloidosis: Clinical features, pathogenesis, diagnosis, and treatment. Turk Patoloji Derg 40: 1-9, 2024.
34. Yang S, Pei T, Wang L, Zeng Y, Li W, Yan S, Xiao W and Cheng W: Salidroside alleviates renal fibrosis in SAMP8 mice by inhibiting ferroptosis. Molecules 27: 8039, 2022.
35. Wang Y, Liao J, Luo Y, Li M, Su X, Yu B, Teng J, Wang H and Lv X: Berberine alleviates doxorubicin-induced myocardial injury and fibrosis by eliminating oxidative stress and mitochondrial damage via promoting Nrf-2 pathway activation. Int J Mol Sci 24: 3257, 2023.
36. Li D, Guo YY, Cen XF, Qiu HL, Chen S, Zeng XF, Zeng Q, Xu M and Tang QZ: Lupeol protects against cardiac hypertrophy via TLR4-PI3K-Akt-NF-κB pathways. Acta Pharmacol Sin 43: 1989-2002, 2022.
37. Jäntti T, Tarvasmäki T, Harjola VP, Parissis J, Pulkki K, Javanainen T, Tolppanen H, Jurkko R, Hongisto M, Kataja A, *et al*: Hypoalbuminemia is a frequent marker of increased mortality in cardiogenic shock. PLoS One 14: e0217006, 2019.
38. Ren B, Feng J, Yang N, Guo Y, Chen C and Qin Q: Ginsenoside Rg3 attenuates angiotensin II-induced myocardial hypertrophy through repressing NLRP3 inflammasome and oxidative stress via modulating SIRT1/NF-κB pathway. Int Immunopharmacol 98: 107841, 2021.
39. Frangogiannis NG: Cardiac fibrosis: Cell biological mechanisms, molecular pathways and therapeutic opportunities. Mol Aspects Med 65: 70-99, 2019.
40. Brilla CG: Renin-angiotensin-aldosterone system and myocardial fibrosis. Cardiovasc Res 47: 1-3, 2000.
41. Töx U and Steffen HM: Impact of inhibitors of the Renin-Angiotensin-aldosterone system on liver fibrosis and portal hypertension. Curr Med Chem 13: 3649-3661, 2006.
42. Wang J, Guo R, Ma X, Wang Y, Zhang Q, Zheng N, Zhang J and Li C: Liraglutide inhibits AngII-induced cardiac fibroblast proliferation and ECM deposition through regulating miR-21/PTEN/PI3K pathway. Cell Tissue Bank 24: 125-137, 2023.